

Preparation of thermal coherent state and its role in quantum thermometry

Asghar Ullah,^{1,*} M. Tahir Naseem,^{2,†} and Özgür E. Müstecaplıoğlu^{1,3,4,‡}

¹*Department of Physics, Koç University, 34450 Sarıyer, Istanbul, Türkiye*

²*Faculty of Engineering Science, Ghulam Ishaq Khan Institute of Engineering Sciences and Technology, Topi 23640, Khyber Pakhtunkhwa, Pakistan*

³*Faculty of Engineering and Natural Sciences, Sabancı University, Tuzla, Istanbul 34956, Türkiye*

⁴*TÜBİTAK Research Institute for Fundamental Sciences, 41470 Gebze, Türkiye*

(Dated: December 27, 2023)

The unavoidable interaction between thermal environments and quantum systems typically leads to the degradation of the quantum coherence, which can be fought against by reservoir engineering. We propose that a thermal coherent state can be realized using a thermally driven two-level system longitudinally coupled to a resonator. Using the master equation approach to describe the open system dynamics, we obtain the steady-state solution of the master equation for the two-level system and resonator. We find that the state of the resonator is a thermal coherent state, while the two-level system remains thermal. This observation is verified by evaluating the second-order correlation coefficient and photon number statistics of the resonator. Moreover, we reveal the potential benefits of employing the thermal coherent state of the resonator in quantum thermometry. In this context, the resonator functions as a probe to measure the unknown temperature of a bath mediated by a two-level system, strategically bridging the connection between the two. Our findings elucidate that using an ancilla-assisted probe may enhance precision and broaden the applicable temperature range.

I. INTRODUCTION

Quantum coherence is a fundamental concept in quantum mechanics related to the superposition of quantum states. Quantum coherence is a crucial resource that underpins many potential advantages of quantum technologies over classical [1–7]. Quantum coherence is utilized as a resource to enhance the performance of several tasks, such as quantum information processing [8, 9], quantum sensing and metrology [10–15], quantum computing [16], and energy harvesting [17, 18]. In the context of thermodynamics, quantum coherence was shown to be a promising candidate for the optimal charging of quantum batteries [19–25], enhancing the efficiency of heat engines and thermal machines [26–30].

Coherent states are minimal uncertainty states that describe the maximum coherence and classical behavior [31]. These states play a pivotal role in quantum physics, serving as fundamental tools for understanding quantum phenomena, quantum information processing, and the exploration of quantum optics [32, 33]. A thermal coherent state generalizes the notion of a coherent state to finite temperatures. By definition, it is a state that is produced by a thermalization operation applied to a displaced (coherent) state [33–36]. A few physical models have been proposed to prepare thermal coherent states (TCSs); for example, a superposition of displaced thermal states can be obtained via the resonant interaction of a two-level atom with a cavity field [37]. The TCS can be generated by quantum state engineering using an on-off detector scheme by pumping a nonlinear crystal with the help of a pump beam [38]. An incident signal is a thermal field mixed with a vacuum field that results in conditional TCS. A probabilistic quantum amplifier can also produce a TCS using a thermal noise source

and a photon number subtraction scheme [39, 40]. TCSs have been extensively studied in thermofield theory. The formalism of thermofield theory permits a more comprehensive formulation of the uncertainty relations, which include the effects of both quantum and thermal fluctuations [41, 42]. The TCSs can be particularly interesting as they saturate the generalized uncertainty relations, as regular coherent states do for the Heisenberg uncertainty relations. Recently, displaced thermal baths have been found to play a significant role in generating steady-state entanglement between two nitrogen-vacancy centers in a diamond host on an ultrathin yttrium iron garnet strip [43].

Gaussian states are continuous variable states that exhibit the Gaussian probability in phase space and are fully characterized by their mean values and covariance matrices. Gaussian states in continuous-variable systems play a key role in the progress of quantum information and quantum metrology because of simple analytical tools and readily available experimental setups [44, 45]. Their versatility makes them suitable for tasks involving secret quantum key distribution and quantum simulation [46–48]. Recently, continuous variable Gaussian systems have attracted much attention for performing low-temperature estimation tasks [45, 49–51]. It is worth noting that, in temperature estimation, finding quantum Fisher information (QFI) and optimal measurements is very demanding. It requires different techniques that depend on the scheme, system dynamics, and the parameter of interest. Yet, one can easily find them for the Gaussian systems. In multiparameter Gaussian quantum metrology, quantum Cramer-Rao bounds can still be saturated asymptotically for the estimation of multiparameters encoded in the multimode Gaussian states [45, 49, 52].

Quantum thermometry using a single qubit as a thermal probe represents a pivotal model with distinctive significance and practical applications [53, 54]. However, single-qubit probes are inherently limited to estimating only a single temperature. To overcome this limitation and estimate multiple

* aullah21@ku.edu.tr

† mnaseem16@ku.edu.tr

‡ omustecap@ku.edu.tr

temperatures, a qubit probe can be coupled with a network of ancilla qubits [15]. However, such networks demand precisely identical qubits with specific engineered anisotropic interactions [55]. Therefore, presenting readily available physical setups, like the coupled qubit-resonator model for quantum thermometry, becomes crucial, demonstrating potential feasibility for experimental implementation [56]. This coupled system retains the same ability to estimate multiple temperatures precisely, hence enhancing the temperature estimation range.

In this paper, we propose a theoretical model for preparing a TCS, which is a single-mode Gaussian state. The proposed model consists of a two-level system (qubit) coupled longitudinally to a resonator [57–62]. In addition, the qubit is also coupled to a thermal bath. Using the master equation approach, we derive the combined steady state of the qubit and resonator. We note that while the qubit remains in a thermal state, the final state of the resonator is TCS. To validate the coherence and thermal nature of the resonator state, we analyze the state’s photon statistics, including the second-order correlation coefficient and photon number distribution. In this scheme, the qubit encodes the temperature information of the thermal bath into the resonator state. A similar process of encoding a qubit into the energy levels of an oscillator is a subject of significant interest. Particularly, Gottesmann-Kitaev-Preskill states are utilized as an error correction technique [63], and this approach extends across various quantum platforms to enhance resilience against thermal noise [64–68].

We take advantage of this TCS and investigate the role of the TCS of the resonator in temperature estimation. We use the resonator as a probe to estimate the temperature of a thermal bath. Due to the Gaussian nature of the probe state, we can analytically calculate the propagation error and QFI as relevant figures of merit. The thermometer allows us to probe more than one temperature with high precision because of the judicious choice of controlled parameters. It is important to highlight that the precision enhancement obtained using TCS of the resonator doesn’t require degeneracy in the excited states of the probe [69, 70] or the need for external control drive [71, 72]. This makes the current scheme more practical in its precision improvement. We further investigate suboptimal measurements, in particular position and momentum measurements. The relative temperature error can be observed with high precision using quadrature measurements. The current setup closely resembles that in Ref. [73], with the key distinction being that the qubit, in their case, acts as a working fluid interacting with both a hot and a cold bath. Additionally, the qubit is coupled to a resonator (referred to as a piston in their terminology). The primary objective of their work is to explore quantum states as thermodynamic resources, aiming to use them as effective tools for controlling and enhancing the efficiency of heat machines.

The rest of the paper is organized as follows: In Sec. II, we present the model system, and after diagonalizing the Hamiltonian, we write the master equation of the system. The results of this study are presented in Sec. III, where we discuss the preparation of TCS and characterize its properties using the second-order correlation function and occupation proba-

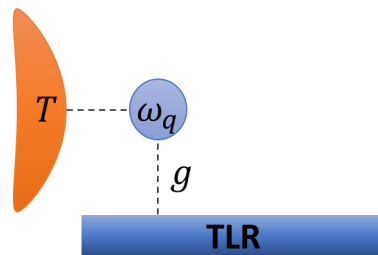


FIG. 1. Model description. We consider a TLS; for example, in the current study, a qubit of frequency ω_q is coupled longitudinally to a resonator of frequency ω_R . In addition, the qubit is also coupled to a thermal bath of temperature T . The qubit-resonator coupling is represented by g . We will observe the thermal effects of the bath in the resonator via qubit.

bility. In Sec. IV, we discuss the advantageous application of a thermal coherent state that can enhance and broaden the range of thermometry precision. Finally, we conclude the paper in Sec. V. In Appendix A, we present the results obtained from numerical simulations and compare them with the analytical calculations. The discussion on the relative error in temperature estimation is given in Appendix B.

II. MODEL AND SYSTEM DYNAMICS

We consider a two-level system (TLS), such as a qubit interacting longitudinally with a single-mode bosonic resonator field. In addition, the qubit is coupled to a thermal bath of temperature T as depicted in Fig. 1. The Hamiltonian of the system of interest is given by (we work in the units where $\hbar = 1 = k_B$ throughout this study) [74–77]

$$\hat{H} = \frac{\omega_q}{2} \hat{\sigma}_z + \omega_R \hat{a}^\dagger \hat{a} + g \hat{\sigma}_z (\hat{a} + \hat{a}^\dagger), \quad (1)$$

where g is the coupling strength between the qubit and resonator, ω_q and ω_R are the frequencies of the qubit and resonator, respectively, and $\hat{\sigma}_i (i = 1, 2, 3)$ are the Pauli operators of the qubit. The bosonic creation (annihilation) operator of the resonator is represented by $\hat{a}^\dagger (\hat{a})$. The longitudinal coupling between the resonator and the qubit has been implemented in circuit QED [76, 77]. This coupling has also been realized for a superconducting flux qubit coupled off resonantly to a transmission line resonator, offering advantages such as enhanced qubit lifetimes, high-fidelity measurements, entanglement over longer distances, and the generation of important microwave photon states for quantum communication [56, 78]. Another mechanism utilizes strain coupling between nitrogen-vacancy centers and a diamond mechanical nanoresonator to enable long-range spin-spin interactions [79]. It is also utilized for reversible information transfer between superconducting qubits and ultracold atoms using a microwave resonator [80]. This model has also been used to predict and describe phonon blockade in a nanomechanical resonator coupled to a Cooper-pair box (i.e., a charge

qubit) for observing strong antibunching and sub-Poissonian phonon-number statistics [74, 81].

In our setup, the qubit is coupled to a multimode bosonic bath, which is modeled as ensembles of harmonic oscillators and described by the Hamiltonian

$$\hat{H}_B = \sum_k \omega_k \hat{b}_k^\dagger \hat{b}_k, \quad (2)$$

and the system-bath interaction has the following form

$$\hat{H}_I = \sum_k \gamma_k \hat{\sigma}_x (\hat{b}_k + \hat{b}_k^\dagger), \quad (3)$$

where $\hat{b}(\hat{b}^\dagger)$ is the annihilation (creation) bosonic operator of the k -th bath modes with $[\hat{b}_k, \hat{b}_{k'}^\dagger] = \delta_{k,k'}$, and γ_k refers to the coupling strength between the k -th bath mode and qubit. To derive the Master equation, we first diagonalize the Hamiltonian given in Eq. (1) with the aid of the following unitary transformation

$$\hat{U} = e^{-\theta \hat{\sigma}_z (\hat{a}^\dagger - \hat{a})}, \quad (4)$$

where $\theta := g/\omega_R$. After performing the unitary transformation, the diagonalized Hamiltonian takes the following form

$$\tilde{H} = \hat{U} \hat{H} \hat{U}^\dagger = \frac{\omega_q}{2} \tilde{\sigma}^+ \tilde{\sigma}^- + \omega_R \tilde{a}^\dagger \tilde{a} - \frac{g^2}{\omega_R}. \quad (5)$$

The frequencies of the qubit and bosonic field modes are unaffected by the longitudinal coupling. The transformed operators are given as

$$\tilde{\sigma}^- = \hat{U} \hat{\sigma}^- \hat{U}^\dagger = \hat{\sigma}^- e^{-\theta(\hat{a}^\dagger - \hat{a})}, \quad (6)$$

$$\tilde{a} = \hat{U} \hat{a} \hat{U}^\dagger = \hat{a} - \theta \hat{\sigma}_z. \quad (7)$$

The master equation can be derived by transforming these operators into the interaction picture followed by the standard Born-Markov and secular approximations. The resulting form of the master equation within the first order expansion for θ in Eq. (6) is written by [73, 75, 82]

$$\begin{aligned} \frac{d\tilde{\rho}}{dt} = & -i[\tilde{H}, \tilde{\rho}] + \mathcal{G}(\omega_q) \mathcal{D}[\tilde{\sigma}^-] + \mathcal{G}(-\omega_q) \mathcal{D}[\tilde{\sigma}^+] \\ & + \theta^2 \{ \mathcal{G}(\omega_q - \omega_R) \mathcal{D}[\tilde{\sigma}^- \tilde{a}^\dagger] + \mathcal{G}(-\omega_q + \omega_R) \mathcal{D}[\tilde{\sigma}^+ \tilde{a}] \\ & + \mathcal{G}(\omega_q + \omega_R) \mathcal{D}[\tilde{\sigma}^- \tilde{a}] + \mathcal{G}(-\omega_q - \omega_R) \mathcal{D}[\tilde{\sigma}^+ \tilde{a}^\dagger] \}. \end{aligned} \quad (8)$$

Here $\mathcal{D}[\hat{x}]$ ($\hat{x} \equiv \hat{a}, \hat{a}^\dagger, \sigma^\pm$) is the Lindblad dissipator which is defined as

$$\mathcal{D}[\hat{x}] = \hat{x} \hat{\rho} \hat{x}^\dagger - \{\hat{\rho}, \hat{x}^\dagger \hat{x}\} / 2, \quad (9)$$

where $\{\hat{A}, \hat{B}\} = \hat{A} \hat{B} + \hat{B} \hat{A}$ represents the anti-commutation relation between two quantum operators. The bath spectral response function in Eq. (8) is given by

$$\mathcal{G}(\omega) = \begin{cases} \gamma(\omega)(1 + \bar{n}(\omega)), & \text{if } \omega > 0, \\ \gamma(|\omega|) \bar{n}(|\omega|), & \text{if } \omega < 0, \end{cases} \quad (10)$$

where $\gamma(\omega)$ is the coupling strength between system and bath and $\bar{n}(\omega) := 1/(e^{\omega/T} - 1)$ is the average photon number of the bath.

III. RESULTS

A. Preparation of thermal coherent state

The steady-state solution of the global Master equation (8) is given by

$$\tilde{\rho}_G = \tilde{\rho}_{th}^{(q)} \otimes \tilde{\rho}_{th}^R, \quad (11)$$

where $\tilde{\rho}_{th}^{(q)}$ and $\tilde{\rho}_{th}^R$ are the qubit and resonator thermal density matrices, respectively. Above Eq. (11) holds under the Born-Markov approximations employed during the derivation of the master equation Eq. (8). The comparison between Eq. (11) and the numerical solution of the master equation (8) is given in Appendix A. Introducing higher-order terms in θ in the expansion of Eq. (6) results in additional dissipative terms in the master equation (8). Notably, these additional dissipative channels do not change the steady state (Eq. (11)) of the system. This observation holds true under the assumption of weak coupling with a thermal bath, where the system is expected to approach a thermal state in accordance with the general principles of statistical mechanics [83]. This is verified by computing the fidelity between the density matrix given in (11) and the numerical solution of the master equation considering higher order terms in θ presented in Appendix A.

To bring the global thermal state $\tilde{\rho}_G$ to the local basis, we first employ the back unitary transformation given in Eq. (4). Subsequently, we apply partial trace over the qubit state to get the desired state of the resonator in the local basis, which reads as

$$\hat{\rho}^{(R)} = \text{Tr}_q[\hat{U} \tilde{\rho}_G \hat{U}^\dagger] = \text{Tr}_q[\hat{U} \tilde{\rho}_{th}^{(q)} \otimes \tilde{\rho}_{th}^R \hat{U}^\dagger]. \quad (12)$$

After performing the partial trace, the resulting state of the resonator is finally given as

$$\hat{\rho}^{(R)} = e^{-\alpha(\hat{a}^\dagger - \hat{a})} \hat{\rho}_{th}^{(R)} e^{+\alpha(\hat{a}^\dagger - \hat{a})}, \quad (13)$$

where $\hat{\rho}_{th}^{(R)}$ is the thermal state of the resonator, i.e., $\hat{\rho}_{th}^{(R)} = \mathcal{Z}^{-1} \sum_n e^{\beta \omega_R \hat{a}^\dagger \hat{a}} |n\rangle \langle n|$ with \mathcal{Z} being the partition function and $\beta := 1/k_B T$ being the inverse temperature. In Eq. (13), the parameter α obtained after performing the partial trace over qubit degrees of freedom is given by

$$\alpha = \theta \tanh\left(\frac{\omega_q}{2T} + \theta\right). \quad (14)$$

The temperature-dependent behavior of α is shown in Fig. 2(b) as a function of T that decays to zero at higher temperatures. The density matrix obtained for the resonator in the local basis (see Eq. (13)) has the form of a thermal coherent state $\hat{D}(\alpha) \hat{\rho}_{th} \hat{D}^\dagger(\alpha)$ with displacement operator defined as $\hat{D}(\alpha) = e^{-(\alpha^* \hat{a} - \alpha \hat{a}^\dagger)}$ and α is in general a complex number. However, in our case, it is a real number given by Eq. (14). Generally, a thermal coherent state is obtained if a thermal state is displaced by an amount of α in phase space. We can obtain the normally ordered form of the thermal coherent state of the resonator such that

$$\hat{\rho}^{(R)} = \frac{1}{\sqrt{\mu}} e^{-w[(\hat{a}^\dagger + \alpha)(\hat{a} + \alpha)]}, \quad (15)$$

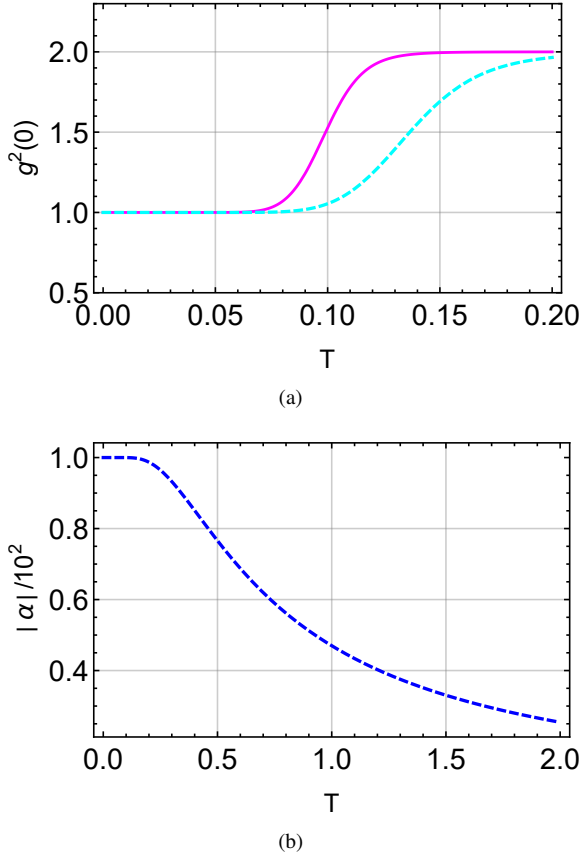


FIG. 2. (a). The second-order correlation coefficient $g^2(0)$ for the steady state of the resonator as a function of bath temperature T . The solid red and cyan dashed curves are for $g = 0.01$ and $g = 0.04$, respectively. (b). The absolute value of $\alpha = g\langle\hat{\sigma}^z\rangle/\omega_R$ is plotted against T . The other parameters are $g = 0.01$, $\omega_q = 1$, and $\omega_R = 1$.

where $\mu := (\bar{n} + 1)^2$ and $w := \omega_R/k_B T$.

Photon statistics: We employ a zero-time, second-order correlation function for investigating the coherence properties of the resonator steady state. The second-order correlation function provides information on the sub-Poissonian and super-Poissonian statistics of the photon field, and it is given by [84]

$$g^2(0) = \frac{\langle\hat{a}^\dagger\hat{a}^\dagger\hat{a}\hat{a}\rangle}{(\langle\hat{a}^\dagger\hat{a}\rangle)^2}. \quad (16)$$

After calculating the average photon number $\langle\hat{n}\rangle = \langle\hat{a}^\dagger\hat{a}\rangle$ and $\langle\hat{a}^\dagger\hat{a}^\dagger\hat{a}\hat{a}\rangle$, the second order correlation coefficient evaluates to

$$g^2(0) = \frac{\alpha^4 + 2\bar{n}^2 + 4\alpha^2\bar{n}}{(\bar{n} + \alpha^2)^2}. \quad (17)$$

In the case of a Poisson distribution, $g^2(0) = 1$, which means that photons in coherent states are uncorrelated, while for $g^2(0) = 2$, the photons are correlated or bunched. If the value of $g^2(0)$ is less than 1, we describe the photon field's statistics as sub-Poissonian, meaning that the state is nonclassical. If the numerical value of the second-order coherence coefficient falls within the range $1 < g^2(0) < 2$, we categorize the state of the resonator as a thermal coherent state.

We plot $g^2(0)$ and α as a function of bath temperature T for different values of the coupling strength g in Fig. 2.

The results suggest that at lower temperatures, the state of the resonator adheres to Poissonian statistics. However, as the temperature of the thermal bath increases, the degree of coherence in the photon field decreases. Another factor affecting the distribution is the coupling strength between the resonator and qubit; stronger coupling results in a slower decrease in the coherence as bath temperature increases. A comparison between the analytical mean photon number $\langle\hat{a}^\dagger\hat{a}\rangle$, zero mean second-order coherence function $g^2(0)$ and numerical results obtained from the master equation (8) is presented in Appendix A.

Occupation probability: Every optical field possesses a crucial characteristic known as the photon number distribution (PND), which describes the probability of finding the specific number of photons within the field. The PND provides a fundamental understanding of the nature of the optical field, including its coherence, statistical properties, and quantum behavior. To calculate the photon number distribution of a thermal coherent state, it is convenient to write the P-function representation of the thermal state

$$\rho_{th} = \frac{1}{\pi\bar{n}} \int e^{-|\alpha|^2/\bar{n}} |\alpha\rangle\langle\alpha| d^2\alpha, \quad (18)$$

where $\bar{n} = 1/(e^{\omega_R/T} - 1)$ is the mean photon number of the thermal field. In the Fock basis, the thermal coherent state reads as

$$\begin{aligned} \rho^{(R)} &= \frac{1}{\pi\bar{n}} \int e^{-|\alpha|^2/\bar{n}} |\alpha + \alpha'\rangle\langle\alpha + \alpha'| d^2\alpha \\ &= \frac{1}{\pi\bar{n}} \sum_{n,m} \int e^{-|\alpha|^2/\bar{n}} e^{-|\alpha+\alpha'|^2} \frac{(\alpha + \alpha')^n (\alpha + \alpha')^m}{\sqrt{m!}\sqrt{n!}} \\ &\quad \times |n\rangle\langle m| d^2\alpha. \end{aligned} \quad (19)$$

The probability of finding n photons in a quantum state described by the density operator $\rho^{(R)}$ can be calculated by taking the projection over the thermal coherent state of the resonator, which reads as

$$P^{(R)}(n) = \text{Tr}(\rho^{(R)} |n\rangle\langle n|). \quad (20)$$

The state of the resonator takes the following form:

$$P^{(R)}(n) = \frac{1}{\pi\bar{n}} \sum_n \int d^2\alpha e^{-|\alpha|^2/\bar{n}} e^{-|\alpha+\alpha'|^2} \frac{(\alpha + \alpha')^{2n}}{n!}. \quad (21)$$

To visualize the coherence in the steady state of the resonator, the PND, or occupation probability, of the state of the resonator is shown in Fig. 3. This indicates that as we increase the coupling strength g , the probability distribution changes from thermal to coherent, as indicated in Fig. 3.

Multimode resonator: To investigate further, we consider a multimode resonator coupled to a qubit. The Hamiltonian of this is given by

$$\hat{H} = \frac{\omega_q}{2} \hat{\sigma}_z + \sum_i \omega_i \hat{a}_i^\dagger \hat{a}_i + \sum_i g_i \hat{\sigma}_z (\hat{a}_i^\dagger + \hat{a}_i), \quad (22)$$

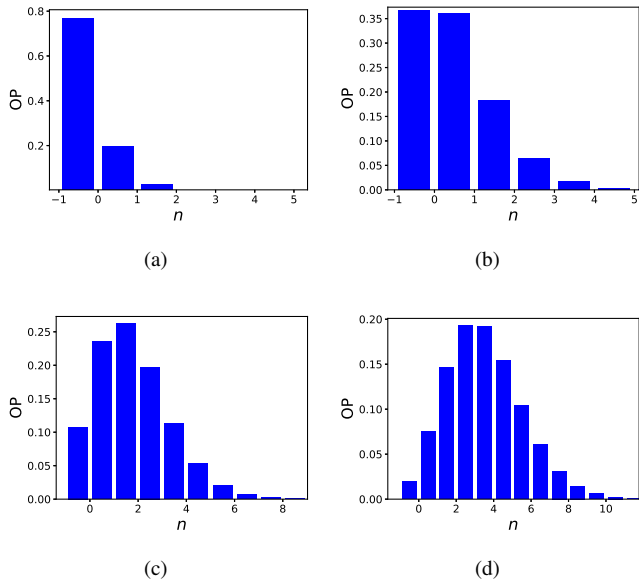


FIG. 3. [(a)–(d)] The occupation probability (OP) of the resonator state with respect to the occupation number of the Fock states n for $\omega_q = 1$, $\omega_R = 0.4$, and $T = 0.1$. The distributions are for different values of coupling strengths between qubit and resonator, such as: (a), $g = 0.04$ (b), $g = 0.2$ (c), $g = 0.4$ and (d), $g = 0.6$.

where g_i is the coupling strength between the qubit and each resonator mode of frequency ω_i . In the case of identical resonator modes, where all the modes have the same frequency ω_i and coupling strengths g_i , the steady states for all modes have the same second-order correlation coefficient $g_1^2(0) = g_i^2(0)$. We now assume that all the modes have different frequencies and coupling strengths. Therefore, the thermal coherent state of the resonator takes the following form:

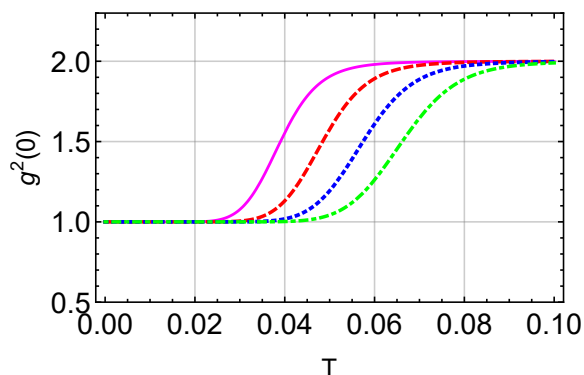


FIG. 4. Second order correlation coefficient $g^2(0)$ as function of bath temperature T for different values of frequencies ω_i : $\omega_1 = 0.3$ (solid magenta line), $\omega_2 = 0.4$ (dashed red line), $\omega_3 = 0.5$ (dotted blue line), and $\omega_4 = 0.6$ (dot-dashed green line). The other parameters are $\omega_q = 1$ and $g_1 = g_2 = g_3 = g_4 = 0.01$.

$$\hat{\rho}_i^{(R)} = \frac{1}{\sqrt{\mu_i}} \exp[-w_i \{(\hat{a}_i + \alpha_i)(\hat{a}_i^\dagger + \alpha_i)\}], \quad (23)$$

where μ_i and w_i are defined in Sec. II. The second-order correlation coefficient for the resonator having i -th modes can be written as

$$g_i^2(0) = \frac{\alpha_i^4 + 2\bar{n}_i^2 + 4\bar{n}_i\alpha_i^2}{(\bar{n}_i + \alpha_i^2)^2}, \quad (24)$$

where α_i is given in Eq. (14). We plot the second-order correlation coefficient $g^2(0)$ for various resonator modes as a function of bath temperature. We assume identical coupling strengths but different frequencies of the modes.

IV. THERMOMETRY WITH TCS

In this section, we delve into the efficacy of TCS in quantum thermometry. To ensure clarity, we revisit fundamental concepts in quantum parameter estimation. We propose feasible observables by measuring position and momentum operators using the resonator's Gaussian state. Finally, we exploit the Gaussian formalism to calculate QFI and classical Fisher information of TCS from the covariance matrix and compare the precision obtained by these two. Employing the error propagation method, we assess the relative error in temperature, which is an alternative method for precision (see Appendix B for detail).

A. Fundamental concepts in thermometry

To begin with, we review some fundamental concepts that are used in quantum thermometry. We know that temperature is a parameter and not a quantum observable; therefore, it can be estimated from the measurements on the probe that is the resonator in our scheme. The choice of measurement influences the accuracy of estimation; for example, in the most general case, the positive operator value measure (POVM) and an estimator \hat{T} constructed from the measurement data turn these measurements into temperature estimation. Therefore, we will use the local parameter estimation theory to quantify the precision of estimation [85]. A central quantity in parameter estimation theory is the QFI, which has a lower bound on the fluctuations of any unbiased estimator. The fluctuations in such estimators obey the Cramér-Rao bound, such as [86, 87]

$$\Delta T \geq 1/\sqrt{n\mathcal{F}_c(T)}, \quad (25)$$

where n is the number of measurement outcomes and $\mathcal{F}_c(T)$ is the classical Fisher information with respect to the unknown parameter T and associated with the particular choice of measurement and is given by

$$\mathcal{F}_c(T) = \int dx p(x|T) [\partial_T \ln p(x|T)]^2, \quad (26)$$

where $\partial_T := \partial/\partial T$ is the partial derivative with respect to T and $p(x|T)$ denotes the conditional probability for an output

measurement x given the unknown parameter T . The QFI is obtained by optimizing classical Fisher information upon all the possible POVM ($\hat{\Pi}(x)$) operators to get an ultimate precision bound and is defined as [85]

$$\mathcal{F}_Q(T) = \text{Tr}[\partial_T \rho_T L_T] = \text{Tr}[\rho_T L_T^2]. \quad (27)$$

The hermitian symmetric logarithmic derivative operator L_T is defined by the equation $2\partial_T \rho_T = L_T \rho_T + \rho_T L_T$. The measurements attaining QFI can be optimal if the estimation error has a lower bound, which is given by the quantum Cramér-Rao lower bound inequality

$$\Delta T \geq 1/\sqrt{n\mathcal{F}_Q(T)}. \quad (28)$$

Therefore, the maximum information obtained from the repeated measurements of state $\rho(T)$ can be quantified by QFI. Using the explicit form of SLD [85], one can write QFI as

$$\mathcal{F}_Q(T) = 2 \sum_{j,k} \frac{|\langle \phi_j | \partial_T \rho_T | \phi_k \rangle|^2}{\lambda_j + \lambda_k}, \quad (29)$$

where ϕ_j, ϕ_k and λ_j, λ_k are the eigenvectors and eigenvalues, respectively. This definition of QFI will help us in our numerical simulation during the study.

B. Results

Quantum Fisher information: It is essential to emphasize that the TCS is obtained by solving Eq. (8) under the conditions of weak coupling. To comprehend how much information about T is genuinely contained within the TCS, a profound understanding is needed. Therefore, it is appropriate to calculate QFI for the TCS to evaluate the effectiveness of our scheme in estimating T . Equation 13 is a single-mode Gaussian state, allowing us to utilize the Gaussian formalism for the analytical calculation of QFI. For a given Gaussian quantum state $\hat{\rho}$, the displacement vector is obtained from the first-order moments, while the covariance matrix (CM) can be obtained from the second-order moments, such that

$$\langle \hat{x} \rangle = \text{Tr}(\hat{x} \hat{\rho}), \quad \sigma_{ij} = \{\langle \hat{x}_i, \hat{x}_j \rangle\}_{\hat{\rho}} - \langle \hat{x}_i \rangle_{\hat{\rho}} \langle \hat{x}_j \rangle_{\hat{\rho}}. \quad (30)$$

Thus, the $2n \times 2n$ positive definite matrix refers to the CM σ of the quantum system. The information about the temperature is encoded into the CM. The QFI based on this CM can be calculated via the following expression [88]

$$\mathcal{F}_Q(T) = \frac{\text{Tr}[\sigma_T^{-1}(\partial_T \sigma_T) \sigma_T^{-1}(\partial_T \sigma_T)]}{2(1 + \mu_T)} + 2 \frac{(\partial_T \mu_T)^2}{1 - \mu_T^4}, \quad (31)$$

where $\mu_T = 1/\sqrt{\text{Det} \sigma_T}$ is the purity of the state. A Gaussian state is fully described by two statistical moments, such as the displacement vector and the CM. As an example, a vacuum state with $\bar{n} = 0$ is a Gaussian state whose displacement vector is zero and CM $\sigma = \mathbb{I}/2$, where \mathbb{I} is a 2×2 identity matrix. Similarly, a thermal state, which is the most fundamental,

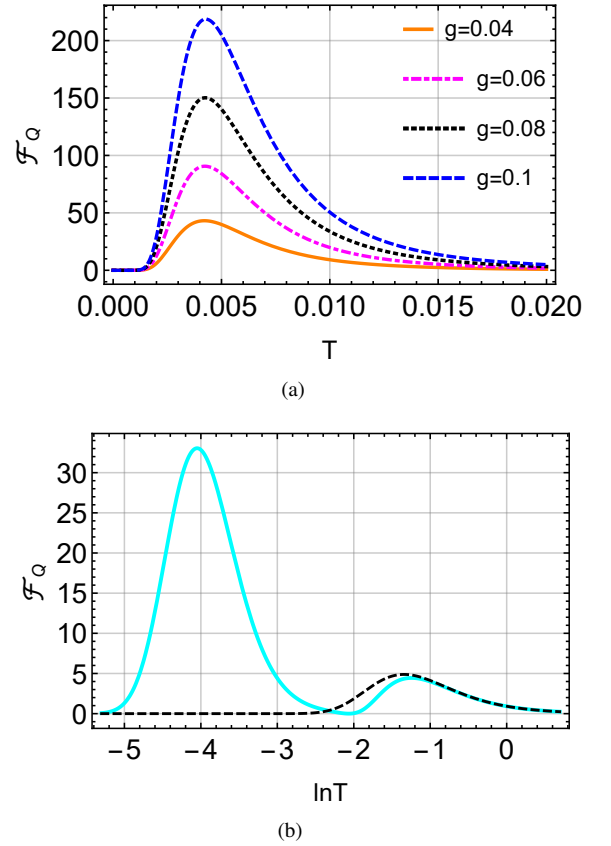


FIG. 5. (a) QFI \mathcal{F}_Q for a TCS of resonator plotted against the bath temperature T for different values of coupling strength g . The frequency of the qubit is set to $\omega_q = 0.01$. The QFI is scaled with the frequency of the resonator ($\omega_R = 1$). (b) We plot \mathcal{F}_Q as a function of T for a TCS of the resonator (cyan) and compare it with the QFI of a thermalized harmonic oscillator (black dashed). The parameters are $\omega_q = 0.04$, $\omega_{osc} = 1$, $g = 0.15$, and $\omega_R = 1$.

is a Gaussian state whose displacement vector is zero while the CM is $\sigma = (2\bar{n} + 1)\mathbb{I}$, where the mean photon number is $\text{Tr}(\hat{\rho} \hat{a}^\dagger \hat{a}) = \bar{n}$ [44]. Using the expression (31), the QFI for the thermal state of a harmonic oscillator of frequency ω_{osc} is $\mathcal{F}_Q^{HO} = \omega_{osc}^2 \text{csch}^2(\omega_{osc}/2T)/4T^4$. This expression is plotted in Fig. 6(b) (black dashed curve) as a function of temperature T . After straight-forward calculation using Eq. (13), one can readily derive the 2×2 covariance matrix σ_T for a TCS, with its temperature-dependent diagonal element is expressed as below

$$\sigma_{11}(T) = \coth\left(\frac{\omega_R}{2T}\right) + 2\theta^2 \tanh^2\left(\frac{g}{\omega_R} + \frac{\omega}{2T}\right). \quad (32)$$

Exploiting the formula of QFI and using the covariance matrix defined earlier, the final expression of QFI takes the fol-

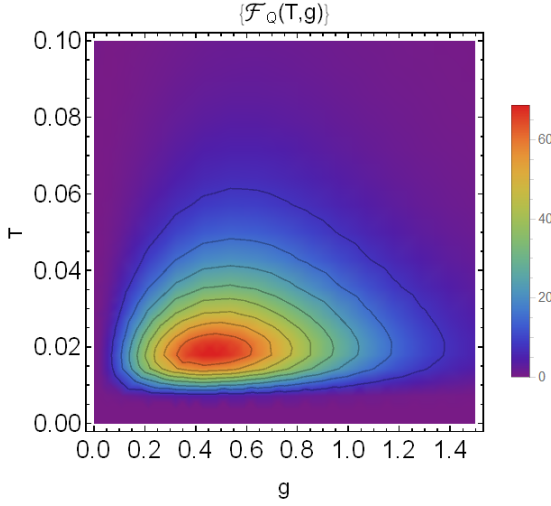


FIG. 6. Density plot of quantum Fisher information $\mathcal{F}_Q(T, g)$ as functions of T and g for fixed values of ω_q and ω_R . The values for the frequencies of the qubit and resonator are $\omega_q = 0.04$ and $\omega_R = 1$, respectively. This plot clearly shows the range of certain values for T and g to be considered so that one gets the desired maximum QFI.

lowing form:

$$\mathcal{F}_Q(T) = \frac{8[\eta(2\alpha + 2\bar{n} + 1) + \zeta(2\bar{n} + 1)]^2}{T^4 \chi^3 \left(1 - \frac{1}{\chi^2}\right)} + \frac{4(\eta - \zeta)^2}{T^4 \left(\frac{1}{\chi} + 1\right) [2(\alpha^2 + \bar{n}) + 1]^2}. \quad (33)$$

For the sake of simplicity, we have introduced some parameters in the above equation, denoted by χ , η , and ζ . The specific values of these parameters are given below

$$\chi = 4\alpha^4 + 4\alpha^2 + 8\bar{n}\alpha^2 + 4\bar{n}^2 + 4\bar{n} + 1, \quad (34)$$

$$\eta = \bar{n}^2 \omega_R e^{\omega_R/T}, \quad \zeta = \alpha \theta \omega_q \operatorname{sech}^2(\Omega).$$

In the above expressions, we defined $\Omega := g/\omega_R + \omega_q/2T$. We use the QFI given in Eq. (33) for the graphical explanation of our results obtained to characterize the precision of temperature estimation. This expression is plotted in Fig. 5(a) with respect to the bath temperature T . We fix the frequencies as $\omega_q = 0.01$ and $\omega_R = 1$ for qubit and resonator, respectively. The QFI is plotted for different values of coupling strength g . One can see that the QFI depends on g for fixed frequencies; as the value of g increases, the precision in T also increases. However, the precision decreases from a weak to a strong coupling regime. It is also important to note that the precision in temperature obtained here is for a very low-temperature regime, as indicated in Fig. 5(a). The robustness of QFI against g can be seen where the QFI $\mathcal{F}_Q(T, g)$ is plotted as functions of T and g as shown in Fig. 6. Without loss of generality, we fixed the qubit and resonator frequencies to be $\omega_q = 0.04$ and $\omega_R = 1$. As evident from the figure, there is a specific domain where the set of controlled parameters (T ,

g) can always be adjusted to maximize the QFI. This could be understood because the master equation is derived considering a weak coupling regime such as $\theta \ll 1$. This is why our results are valid only in the weak coupling regime. A notable advantage of our scheme is that the resonator can probe more than one temperature, as indicated in Fig. 5(b). To better comprehend the results, we plotted the QFI of a harmonic oscillator represented by a black dashed curve for $\omega_{osc} = 1$. This comparison highlights that a two-level quantum system or harmonic oscillator cannot probe more than one temperature. However, the resonator can resolve more than one temperature. Notably, the QFI exhibits two peaks, one at low temperature, whose magnitude can be adjusted by varying the ω_q and g values. The second peak at higher temperatures is almost indistinguishable from that of a harmonic oscillator. It is important to note that we do not require highly degenerate excited states to resolve multiple peaks in QFI [70], a task that can be challenging in practice. An alternative approach to enhancing the upper limit of accuracy in low-temperature estimation involves employing a thermometer characterized by a dynamically controlled multilevel quantum probe in contact with a bath [72].

One can also compute the classical Fisher information \mathcal{F}_C associated with the Gaussian state measurement performed on the resonator that is working as a probe. In addition, this will help us in comparing the QFI \mathcal{F}_Q of the probe with the CFI \mathcal{F}_C . As mentioned earlier, the covariance matrix depends on the parameter T , and the associated classical Fisher information can be evaluated using the formula

$$\mathcal{F}_C(T) = \frac{1}{2} \operatorname{Tr}[\sigma_T^{-1} (\partial_T \sigma_T) \sigma_T^{-1} (\partial_T \sigma_T)]. \quad (35)$$

Therefore, using the above expression, the classical Fisher information becomes

$$\mathcal{F}_C(T) = \frac{4(\eta - \zeta)^2}{T^4 [2(\alpha^2 + n) + 1]^2}. \quad (36)$$

This expression clearly indicates that the QFI surpasses the CFI, as denoted by $\mathcal{F}_Q > \mathcal{F}_C$ in the low-temperature regime.

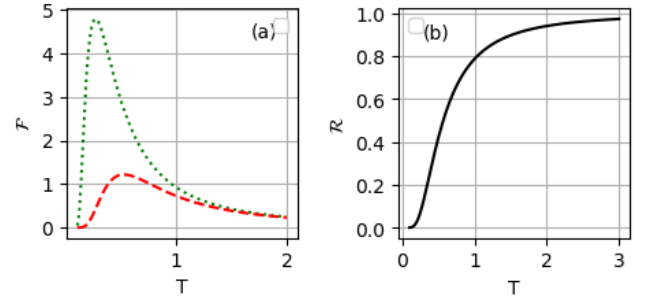


FIG. 7. (a) The classical (red dashed) and quantum (green dotted) Fisher information as a function of T with the coupling strength value $g = 0.02$. (b) Fisher information ratio $\mathcal{R} = \mathcal{F}_C/\mathcal{F}_Q$ as a function of T . The plot is obtained by fixing the parameters to $\omega_q = \omega_R = 1$ and $g = 0.01$.

In Fig 7(b), we compute the Fisher information ratio $\mathcal{R} = \mathcal{F}_C/\mathcal{F}_Q$ as a function of bath temperature T . We fix the parameters to $\omega_q = \omega_R = 1$ and $g = 0.01$. As depicted in the figure, the ratio begins at zero, undergoes an increase, and eventually saturates at higher temperatures. This observation shows that the QFI surpasses the CFI at low temperatures; however, the \mathcal{F}_Q approaches the \mathcal{F}_C as the temperature increases. The CFI (red dashed) and QFI (green dotted) as a function of temperature T for a fixed value of $g = 0.08$ are shown in Fig. 7(a). The QFI \mathcal{F}_Q is 5 times greater than \mathcal{F}_C , such as $\mathcal{F}_Q \approx 5\mathcal{F}_C$. In the strong coupling regime (g), the QFI converges to the CFI very rapidly. The trend in the ratio of Fisher information aligns with the characteristics of the TCS of the resonator. At a high temperature T and strong coupling strength g , the thermal properties of the state dominate the coherent properties, leading to a dominance of classical features and, consequently, the QFI approaching the CFI.

Suboptimal thermometry and feasible measurements: We further study the estimation errors in temperature by exploring more practical observables. Specifically, we focus on individual measurements of either the position or momentum of the TCS of the resonator. We remark that the position and momentum quadratures belong to the Gaussian measurements and are characterized by the covariance matrix. The QFI based on quadrature measurements (\hat{x} or \hat{p}) is given by

$$\mathcal{F}_Q(\hat{x}, T) = \frac{|\partial_T \langle \hat{x}^2 \rangle|^2}{2\langle \hat{x}^2 \rangle^2}. \quad (37)$$

This expression corresponds to the inverse of the error propagation for the observable \hat{x}^2 , and it similarly applies to the measurement of momentum, \hat{p} in our scheme. The analytical expression for QFI based on \hat{x} measurement reads as

$$\mathcal{F}_Q(\hat{x}, T) = \frac{(\eta - 2\xi)^2}{2T^4(2\alpha + \bar{n})^2}. \quad (38)$$

We illustrate the QFI for position measurement \hat{x} in Fig. 8. The figure shows that the QFI displays two peaks for the temperature T and exhibits high sensitivity to the coupling strength (g). The peak at higher temperatures can be modulated by adjusting the value of g , while the low-temperature peak can be controlled by varying the qubit frequency ω_q . Notably, we emphasize that the peak corresponding to high temperatures decreases as g is increased, aligning with the behavior of the TCS of the resonator.

V. CONCLUSION

We investigated the preparation of a thermal coherent state of a resonator coupled to a thermal bath via an ancillary two-level system. In particular, our focus was on a longitudinally coupled qubit to a resonator, which serves as a representative model for a broad category of physical systems [74–77]. The qubit is excited by attaching a thermal bath of temperature T to it. The dynamics of the system is described by a thermodynamically consistent master equation. The steady-state solution of the master equation showed that the state of the

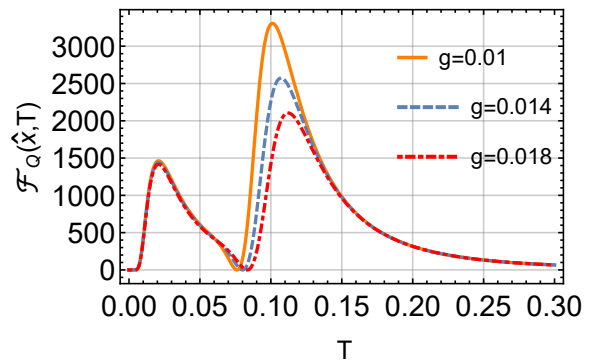


FIG. 8. QFI $\mathcal{F}_Q(\hat{x}, T)$ as a function of T for various values of coupling strength g based on the quadrature measurement \hat{x} . The rest of the parameters are the same as in Fig. 6.

resonator is a thermal coherent state. To quantify its properties, we studied the photon statistics, and the results showed that the TCS follows a Poissonian distribution ($g^2(0) \approx 1$) at low temperatures, indicating the state's coherent properties. However, the photon statistics become super-Poissonian ($g^2(0) > 1$) as the temperature of the bath increases, which confirms the thermal properties of a coherent state.

We take into account the coherent and thermal nature of the TCS of the resonator and use it to estimate the unknown temperature of the thermal bath. For temperature estimation, we consider the resonator as a probe to measure T with the assistance of a qubit attached to the thermal bath. Taking advantage of the Gaussian characteristics of TCS, we employed tools from Gaussian quantum metrology to calculate QFI. Our results indicate that the TCS, within an ancilla-assisted quantum thermometry scheme, not only enhances precision at low temperatures but also broadens the measurable range. Subsequently, our approach can be feasible for practical measurements since we consider temperature estimation based on quadrature observables, such as position and momentum.

Our results may find applications in preserving quantum coherence within a quantum system when exposed to thermal baths [89, 90]. In addition, this coherence can be useful in broadening the range of temperature estimation in ancilla-assisted quantum thermometry schemes [91].

Acknowledgment

This work is supported by the Scientific and Technological Research Council of Türkiye (TÜBİTAK) under grant number 122F371.

Appendix A: Analytical vs numerical results

Including terms up to the second order in θ in the expansion of Eq. (6), the master equation can be formulated under the

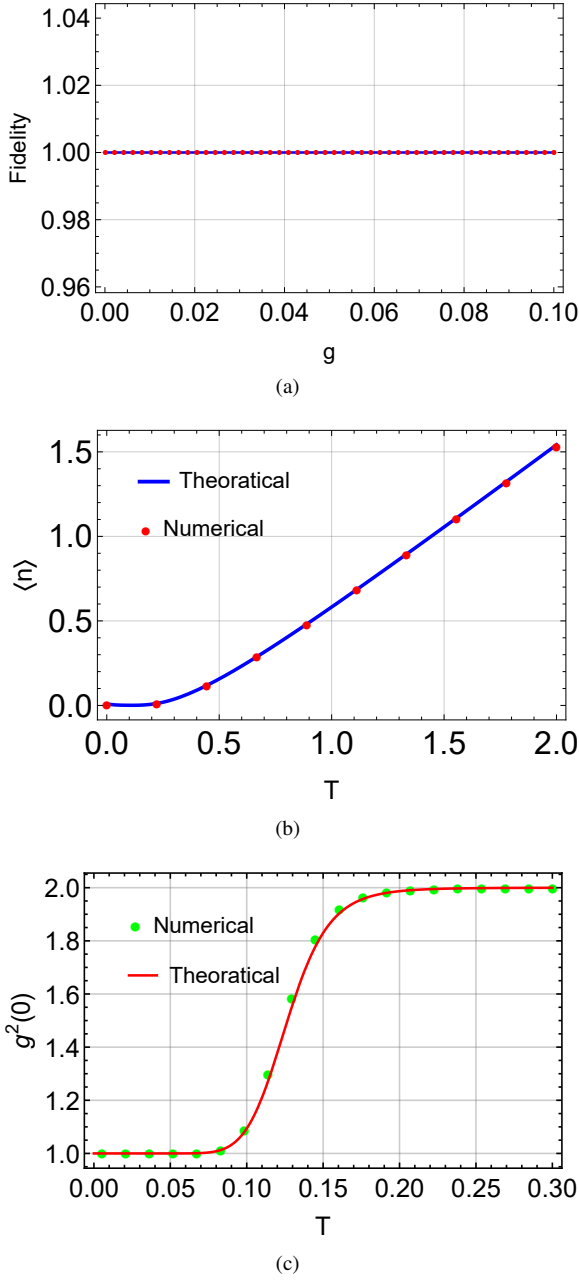


FIG. 9. (a) The fidelity is plotted as a function of the coupling strength g . The solid line corresponds to the numerical solution of the master equation (8). In contrast, the dotted line represents the result obtained from (A1), both compared with the thermal state (11).

(b) The mean photon number $\langle n \rangle$ for TCS with respect to temperature T . The blue curve is plotted using Eq. (B2), and the red dotted curve is obtained with numerical simulations. The parameters considered here are $\omega_q = 0.06$, $g = 0.08$, and $\omega_R = 1$.

(c) Represents the second-order correlation function $g^2(0)$ as a function of temperature T . The parameters are $\omega_q = 1$, $g = 0.03$, and $\omega_R = 1$.

Born-Markov and Secular approximations as [75, 92]

$$\frac{d\tilde{\rho}'}{dt} = -i[\tilde{H}, \tilde{\rho}] + \mathcal{G}(\omega_q)\{\mathcal{D}[\tilde{\sigma}_-] + \theta^3\mathcal{D}[\tilde{\sigma}_-\tilde{a}^\dagger\tilde{a}]\}$$

$$\begin{aligned} &+ \mathcal{G}(-\omega_q)\{\mathcal{D}[\tilde{\sigma}_+] + \theta^3\mathcal{D}[\tilde{\sigma}_+\tilde{a}^\dagger\tilde{a}]\} \\ &+ \sum_{n=1,2} \theta^{n+1} \left\{ \mathcal{G}(\omega_q - n\omega_R)\mathcal{D}[\tilde{\sigma}_-\tilde{a}^{\dagger n}] \right. \\ &+ \mathcal{G}(-\omega_q + n\omega_R)\mathcal{D}[\tilde{\sigma}_+\tilde{a}^n] \\ &+ \mathcal{G}(\omega_q + n\omega_R)\mathcal{D}[\tilde{\sigma}_-\tilde{a}^n] \\ &\left. + \mathcal{G}(-\omega_q - n\omega_R)\mathcal{D}[\tilde{\sigma}_+\tilde{a}^{\dagger n}] \right\}. \end{aligned} \quad (\text{A1})$$

Here, we show that the additional dissipators introduced in Eq. (A1), in comparison to the master equation (8), do not induce changes in the system's steady state as expressed in Eq. (11). This is possible because the system is weakly coupled with a thermal bath, where it is expected to converge to a thermal state following the fundamental principles of statistical mechanics [83]. It is verified by comparing the fidelity

$$\mathcal{F} = (\text{Tr} \sqrt{\sqrt{\tilde{\rho}}\tilde{\rho}'\sqrt{\tilde{\rho}}})^2 \quad (\text{A2})$$

between the thermal state $\tilde{\rho}$ given in Eq. (11) and density matrix $\tilde{\rho}'$ obtained via numerical solution of the master equation (A1).

To confirm our analytical results, we plot the mean photon number $\langle n \rangle$ as a function of T for the resonator state, as shown in Fig. 9. The solid curves are plotted using the analytical expressions in Eq. (B2) and Eq. (17), while the dotted points correspond to results obtained through numerical simulations using the master equation (8). The numerical simulations are performed using open-source packages in QuTiP [93]. We note a quantitative agreement (as evidenced by the overlap of both plots in the figures) between the two methods.

Appendix B: Error propagation method

We calculate the inverse of error propagation, which is an alternative way of characterizing precision. The error propagation to characterize the estimation error for any observable \hat{X} is defined as [52]

$$\delta^2 T_{EP} := \frac{\text{Var}(\hat{X})}{|\partial_T \langle \hat{X} \rangle|^2}. \quad (\text{B1})$$

To estimate the temperature of the bath using the above formula, we need to find the expectation values $\langle \hat{a}^\dagger \hat{a} \rangle$ and $\langle (\hat{a}^\dagger \hat{a})^2 \rangle$. Employing Eq. (13), one can analytically derive these values. Then, the expectation values from the TCS (13) can easily be obtained, and these read as

$$\begin{aligned} \langle \hat{a}^\dagger \hat{a} \rangle &= \bar{n} + \alpha^2, \\ \langle (\hat{a}^\dagger \hat{a})^2 \rangle &= 2\bar{n}^2 + \bar{n}(4\alpha^2 + 1) + \alpha^4 + \alpha^2. \end{aligned} \quad (\text{B2})$$

The variance in the number operator of the TCS has the value

$$\Delta n_{TCS}^2 = \bar{n}(\bar{n} + 1) + (2\bar{n} + 1)\alpha^2. \quad (\text{B3})$$

From the above equations (i.e., Eq. (B2)), it is evident that direct photon detection (with the measurement operator $\langle \hat{a}^\dagger \hat{a} \rangle$)

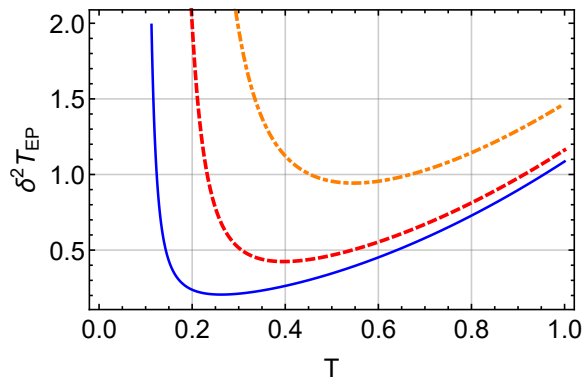


FIG. 10. The uncertainty $\delta^2 T_{EP}$ of T as a function of bath temperature T for different values of coupling strength g . The solid blue, red dashed, and orange dot-dashed curves correspond to $g = 0.01$, $g = 0.2$, and $g = 0.4$, respectively. The other parameters are $\omega_q = 1$ and $\omega_R = 1$.

can be employed for estimating the temperature T of the sample under investigation. By applying the error propagation formula, the uncertainty of $\delta^2 T_{EP}$ can be derived as follows:

$$\delta^2 T_{EP} = \frac{T^4 \eta [2\alpha^2 \sinh(\frac{\omega_R}{T}) + 1]}{\omega_R (\eta - \zeta)^2}, \quad (\text{B4})$$

The behavior of uncertainty $\delta^2 T_{EP}$ as a function of T is shown in Fig. (5). This figure indicates that the uncertainty in T decreases as the coupling strength g between the qubit resonator is decreased from $g = 0.4$ (orange dot-dashed curve) to $g = 0.01$ (blue curve). From this method, we can conclude that the temperature estimation is better within the weak coupling regime.

-
- [1] Lars S. Madsen, Vladyslav C. Usenko, Mikael Lassen, Radim Filip, and Ulrik L. Andersen, “Continuous variable quantum key distribution with modulated entangled states,” *Nat. Commun.* **3**, 1083 (2012).
- [2] Radim Filip, “Quantum interface to a noisy system through a single kind of arbitrary gaussian coupling with limited interaction strength,” *Phys. Rev. A* **80**, 022304 (2009).
- [3] Petr Marek, Radim Filip, and Akira Furusawa, “Deterministic implementation of weak quantum cubic nonlinearity,” *Phys. Rev. A* **84**, 053802 (2011).
- [4] P. Grangier, R. E. Slusher, B. Yurke, and A. LaPorta, “Squeezed-light-enhanced polarization interferometer,” *Phys. Rev. Lett.* **59**, 2153–2156 (1987).
- [5] Shuntaro Takeda, Takahiro Mizuta, Maria Fuwa, Peter van Loock, and Akira Furusawa, “Deterministic quantum teleportation of photonic quantum bits by a hybrid technique,” *Nature* **500**, 315–318 (2013).
- [6] Shota Yokoyama, Ryuji Ukai, Seiji C. Armstrong, Chanond Sornphiphatphong, Toshiyuki Kaji, Shigenari Suzuki, Jun-ichi Yoshikawa, Hidehiro Yonezawa, Nicolas C. Menicucci, and Akira Furusawa, “Ultra-large-scale continuous-variable cluster states multiplexed in the time domain,” *Nat. Photon.* **7**, 982–986 (2013).
- [7] Alexei Ourjoumstev, Rosa Tualle-Brouri, Julien Laurat, and Philippe Grangier, “Generating optical schrödinger kittens for quantum information processing,” *Science* **312**, 83–86 (2006).
- [8] Dirk Bouwmeester and Anton Zeilinger, *The physics of quantum information: basic concepts* (Springer, 2000).
- [9] Samuel L. Braunstein and Peter van Loock, “Quantum information with continuous variables,” *Rev. Mod. Phys.* **77**, 513–577 (2005).
- [10] Girish S Agarwal, *Quantum optics* (Cambridge University Press, 2012).
- [11] Michael A. Taylor and Warwick P. Bowen, “Quantum metrology and its application in biology,” *Phys. Rep.* **615**, 1–59 (2016).
- [12] Zhe-Yu Jeff Ou, *Multi-photon quantum interference*, Vol. 43 (Springer, 2007).
- [13] Luca Pezzè, Augusto Smerzi, Markus K. Oberthaler, Roman Schmied, and Philipp Treutlein, “Quantum metrology with nonclassical states of atomic ensembles,” *Rev. Mod. Phys.* **90**, 035005 (2018).
- [14] L. Podhóra, L. Lachman, T. Pham, A. Lešundák, O. Číp, L. Slodička, and R. Filip, “Quantum non-gaussianity of multiphonon states of a single atom,” *Phys. Rev. Lett.* **129**, 013602 (2022).
- [15] Asghar Ullah, M. Tahir Naseem, and Özgür E. Müstecaplıoğlu, “Low-temperature quantum thermometry boosted by coherence generation,” *Phys. Rev. Res.* **5**, 043184 (2023).
- [16] Andrew Steane, “Quantum computing,” *Rep. Prog. Phys.* **61**, 117 (1998).
- [17] Filippo Caruso, Alex W. Chin, Animesh Datta, Susana F. Huelga, and Martin B. Plenio, “Entanglement and entangling power of the dynamics in light-harvesting complexes,” *Phys. Rev. A* **81**, 062346 (2010).
- [18] Masoud Mohseni, Patrick Rebentrost, Seth Lloyd, and Alan Aspuru-Guzik, “Environment-assisted quantum walks in photosynthetic energy transfer,” *J. chem. Phys.* **129**, 11B603 (2008).
- [19] Ju-Yeon Gyhm, Dominik Šafránek, and Dario Rosa, “Quantum charging advantage cannot be extensive without global operations,” *Phys. Rev. Lett.* **128**, 140501 (2022).
- [20] Stella Seah, Martí Perarnau-Llobet, Géraldine Haack, Nicolas Brunner, and Stefan Nimmrichter, “Quantum speed-up in collisional battery charging,” *Phys. Rev. Lett.* **127**, 100601 (2021).
- [21] F. H. Kamin, F. T. Tabesh, S. Salimi, and Alan C. Santos, “Entanglement, coherence, and charging process of quantum batteries,” *Phys. Rev. E* **102**, 052109 (2020).
- [22] Gian Marcello Andolina, Maximilian Keck, Andrea Mari, Michele Campisi, Vittorio Giovannetti, and Marco Polini, “Extractable work, the role of correlations, and asymptotic freedom in quantum batteries,” *Phys. Rev. Lett.* **122**, 047702 (2019).
- [23] Dario Ferraro, Michele Campisi, Gian Marcello Andolina, Vittorio Pellegrini, and Marco Polini, “High-power collective charging of a solid-state quantum battery,” *Phys. Rev. Lett.* **120**, 117702 (2018).
- [24] Francesco Campaioli, Felix A. Pollock, Felix C. Binder, Lucas Céleri, John Gould, Sai Vinjanampathy, and Kavan Modi, “Enhancing the charging power of quantum batteries,” *Phys. Rev. Lett.* **118**, 150601 (2017).

- [25] Robert Alicki and Mark Fannes, “Entanglement boost for extractable work from ensembles of quantum batteries,” *Phys. Rev. E* **87**, 042123 (2013).
- [26] Marlan O. Scully, Kimberly R. Chapin, Konstantin E. Dorfman, Moochan Barnabas Kim, and Anatoly Svidzinsky, “Quantum heat engine power can be increased by noise-induced coherence,” *Proc. Natl. Acad. Sci.* **108**, 15097–15100 (2011).
- [27] Ali Ü. C. Hardal and Özgür E. Müstecaplıoğlu, “Superradiant quantum heat engine,” *Sci. Rep.* **5**, 12953 (2015).
- [28] Ceren B. Dağ, Wolfgang Niedenzu, Özgür E. Müstecaplıoğlu, and Gershon Kurizki, “Multiatom quantum coherences in micromasers as fuel for thermal and nonthermal machines,” *Entropy* **18** (2016).
- [29] B. Çakmak, A. Manatuly, and Ö. E. Müstecaplıoğlu, “Thermal production, protection, and heat exchange of quantum coherences,” *Phys. Rev. A* **96**, 032117 (2017).
- [30] Kenza Hammam, Heather Leitch, Yassine Hassouni, and Gabriele De Chiara, “Exploiting coherence for quantum thermodynamic advantage,” *New J. Phys.* **24**, 113053 (2022).
- [31] Roy J. Glauber, “Coherent and incoherent states of the radiation field,” *Phys. Rev.* **131**, 2766–2788 (1963).
- [32] John R Klauder and Bo-Sture Skagerstam, *Coherent states: applications in physics and mathematical physics* (World sci., 1985).
- [33] Wei-Min Zhang, Da Hsuan Feng, and Robert Gilmore, “Coherent states: Theory and some applications,” *Rev. Mod. Phys.* **62**, 867–927 (1990).
- [34] R F Bishop and A Vourdas, “Coherent mixed states and a generalised p representation,” *J. Phys. A: Math. Gen.* **20**, 3743 (1987).
- [35] J. Oz-Vogt, A. Mann, and M. Revzen, “Thermal coherent states and thermal squeezed states,” *J. Mod. Opt.* **38**, 2339–2347 (1991).
- [36] Paulina Marian and Tudor A. Marian, “Optimal purifications and fidelity for displaced thermal states,” *Phys. Rev. A* **76**, 054307 (2007).
- [37] Shi-Biao Zheng, “Macroscopic superposition and entanglement for displaced thermal fields induced by a single atom,” *Phys. Rev. A* **75**, 032114 (2007).
- [38] Omar S. Magaña-Loaiza, Roberto de J. León-Montiel, Armando Perez-Leija, Alfred B. U’Ren, Chenglong You, Kurt Busch, Adriana E. Lita, Sae Woo Nam, Richard P. Mirin, and Thomas Gerrits, “Multiphoton quantum-state engineering using conditional measurements,” *npj Quantum Inf.* **5**, 80 (2019).
- [39] Mario A. Usuga, Christian R. Müller, Christoffer Wittmann, Petr Marek, Radim Filip, Christoph Marquardt, Gerd Leuchs, and Ulrik L. Andersen, “Noise-powered probabilistic concentration of phase information,” *Nat. Phys.* **6**, 767–771 (2010).
- [40] Petr Marek and Radim Filip, “Coherent-state phase concentration by quantum probabilistic amplification,” *Phys. Rev. A* **81**, 022302 (2010).
- [41] Raymond F. Bishop and Apostlos Vourdas, “Thermal coherent states, a broader class of mixed coherent states and generalized thermofield dynamics,” *Int. J. Mod. Phys. B* **21**, 2529–2545 (2007).
- [42] A. Mann, M. Revzen, K. Nakamura, H. Umezawa, and Y. Yamanaoka, “Coherent and thermal coherent state,” *J. Math. Phys.* **30**, 2883–2890 (1989).
- [43] Kamran Ullah, Emre Köse, Rawana Yagan, Mehmet C. Onbaşı, and Özgür E. Müstecaplıoğlu, “Steady state entanglement of distant nitrogen-vacancy centers in a coherent thermal magnon bath,” *Phys. Rev. Res.* **4**, 023221 (2022).
- [44] Christian Weedbrook, Stefano Pirandola, Raúl García-Patrón, Nicolas J. Cerf, Timothy C. Ralph, Jeffrey H. Shapiro, and Seth Lloyd, “Gaussian quantum information,” *Rev. Mod. Phys.* **84**, 621–669 (2012).
- [45] Rosanna Nichols, Pietro Liuzzo-Scorpo, Paul A. Knott, and Gerardo Adesso, “Multiparameter gaussian quantum metrology,” *Phys. Rev. A* **98**, 012114 (2018).
- [46] Maciej Lewenstein, Anna Sanpera, Veronica Ahufinger, Bogdan Damski, Aditi Sen(De), and Ujjwal Sen, “Ultracold atomic gases in optical lattices: mimicking condensed matter physics and beyond,” *Advances in Physics* **56**, 243–379 (2007).
- [47] Eleni Diamanti and Anthony Leverrier, “Distributing secret keys with quantum continuous variables: Principle, security and implementations,” *Entropy* **17**, 6072–6092 (2015).
- [48] Miguel Navascués and Antonio Acín, “Security bounds for continuous variables quantum key distribution,” *Phys. Rev. Lett.* **94**, 020505 (2005).
- [49] Zhang Jiang, “Quantum fisher information for states in exponential form,” *Phys. Rev. A* **89**, 032128 (2014).
- [50] Guim Planella, Marina F. B. Cenni, Antonio Acín, and Mohammad Mehboudi, “Bath-induced correlations enhance thermometry precision at low temperatures,” *Phys. Rev. Lett.* **128**, 040502 (2022).
- [51] Safoura S. Mirkhalaf, Mohammad Mehboudi, Zohre Nafari Qaleh, and Saleh Rahimi-Keshari, “Operational significance of nonclassicality in nonequilibrium gaussian quantum thermometry,” (2023), [arXiv:2207.10742 \[quant-ph\]](https://arxiv.org/abs/2207.10742).
- [52] Marina F.B. Cenni, Ludovico Lami, Antonio Acín, and Mohammad Mehboudi, “Thermometry of Gaussian quantum systems using Gaussian measurements,” *Quantum* **6**, 743 (2022).
- [53] Mohammad Mehboudi, Anna Sanpera, and Luis A Correa, “Thermometry in the quantum regime: recent theoretical progress,” *J. Phys. A: Math. Theor.* **52**, 303001 (2019).
- [54] Antonella De Pasquale and Thomas M. Stace, “Quantum thermometry,” in *Thermodynamics in the Quantum Regime: Fundamental Aspects and New Directions* (Springer International Publishing, Cham, 2018).
- [55] Cahit Kargı, M. Tahir Naseem, Tomáš Opatrný, Özgür E. Müstecaplıoğlu, and Gershon Kurizki, “Quantum optical two-atom thermal diode,” *Phys. Rev. E* **99**, 042121 (2019).
- [56] Ze-Liang Xiang, Sahel Ashhab, J. Q. You, and Franco Nori, “Hybrid quantum circuits: Superconducting circuits interacting with other quantum systems,” *Rev. Mod. Phys.* **85**, 623–653 (2013).
- [57] N Etehadı Abarı, A A Rakhubovsky, and R Filip, “Thermally-induced qubit coherence in quantum electromechanics,” *New J. Phys.* **24**, 113006 (2022).
- [58] Yiwen Chu, Prashanta Kharel, William H. Renninger, Luke D. Burkhardt, Luigi Frunzio, Peter T. Rakich, and Robert J. Schoelkopf, “Quantum acoustics with superconducting qubits,” *Science* **358**, 199–202 (2017).
- [59] L. R. Sletten, B. A. Moores, J. J. Viennot, and K. W. Lehnert, “Resolving phonon fock states in a multimode cavity with a double-slit qubit,” *Phys. Rev. X* **9**, 021056 (2019).
- [60] F Rouxinol, Y Hao, F Brito, A O Caldeira, E K Irish, and M D LaHaye, “Measurements of nanoresonator-qubit interactions in a hybrid quantum electromechanical system,” *Nanotechnology* **27**, 364003 (2016).
- [61] Jader P. Santos, Lucas C. Céleri, Gabriel T. Landi, and Mauro Paternostro, “The role of quantum coherence in nonequilibrium entropy production,” *npj Quantum Inf.* **5**, 23 (2019).
- [62] E. Alex Wollack, Agnetta Y. Cleland, Rachel G. Grunenke, Zhaoyou Wang, Patricio Arrangoiz-Arriola, and Amir H. Safavi-Naeini, “Quantum state preparation and tomography of entangled mechanical resonators,” *Nature* **604**, 463–467 (2022).

- [63] Daniel Gottesman, Alexei Kitaev, and John Preskill, “Encoding a qubit in an oscillator,” *Phys. Rev. A* **64**, 012310 (2001).
- [64] Jacob Hastrup and Ulrik L. Andersen, “Protocol for generating optical gottesman-kitaev-preskill states with cavity qed,” *Phys. Rev. Lett.* **128**, 170503 (2022).
- [65] B. M. Terhal and D. Weigand, “Encoding a qubit into a cavity mode in circuit qed using phase estimation,” *Phys. Rev. A* **93**, 012315 (2016).
- [66] Yunong Shi, Christopher Chamberland, and Andrew Cross, “Fault-tolerant preparation of approximate gkp states,” *New J. Phys.* **21**, 093007 (2019).
- [67] Jérémie Guillaud, Joachim Cohen, and Mazyar Mirrahimi, “Quantum computation with cat qubits,” *SciPost Phys. Lect. Notes*, **72** (2023).
- [68] Jacob Hastrup and Ulrik Lund Andersen, “Analysis of loss correction with the gottesman-kitaev-preskill code,” *Phys. Rev. A* **108**, 052413 (2023).
- [69] Luis A. Correa, Mohammad Mehboudi, Gerardo Adesso, and Anna Sanpera, “Individual quantum probes for optimal thermometry,” *Phys. Rev. Lett.* **114**, 220405 (2015).
- [70] Steve Campbell, Marco G Genoni, and Sebastian Deffner, “Precision thermometry and the quantum speed limit,” *Quantum Sci. Technol.* **3**, 025002 (2018).
- [71] Jonas Glatthard and Luis A. Correa, “Bending the rules of low-temperature thermometry with periodic driving,” *Quantum* **6**, 705 (2022).
- [72] Victor Mukherjee, Analia Zwick, Arnab Ghosh, Xi Chen, and Gershon Kurizki, “Enhanced precision bound of low-temperature quantum thermometry via dynamical control,” *Commun. Phys.* **2**, 162 (2019).
- [73] D. Gelbwaser-Klimovsky and G. Kurizki, “Heat-machine control by quantum-state preparation: From quantum engines to refrigerators,” *Phys. Rev. E* **90**, 022102 (2014).
- [74] M. D. LaHaye, J. Suh, P. M. Echternach, K. C. Schwab, and M. L. Roukes, “Nanomechanical measurements of a superconducting qubit,” *Nature* **459**, 960–964 (2009).
- [75] M. Tahir Naseem and Özgür E. Müstecaplıoğlu, “Antibunching via cooling by heating,” *Phys. Rev. A* **105**, 012201 (2022).
- [76] Susanne Richer and David DiVincenzo, “Circuit design implementing longitudinal coupling: A scalable scheme for superconducting qubits,” *Phys. Rev. B* **93**, 134501 (2016).
- [77] Nicolas Didier, Jérôme Bourassa, and Alexandre Blais, “Fast quantum nondemolition readout by parametric modulation of longitudinal qubit-oscillator interaction,” *Phys. Rev. Lett.* **115**, 203601 (2015).
- [78] Alexandre Blais, Ren-Shou Huang, Andreas Wallraff, S. M. Girvin, and R. J. Schoelkopf, “Cavity quantum electrodynamics for superconducting electrical circuits: An architecture for quantum computation,” *Phys. Rev. A* **69**, 062320 (2004).
- [79] S. D. Bennett, N. Y. Yao, J. Otterbach, P. Zoller, P. Rabl, and M. D. Lukin, “Phonon-induced spin-spin interactions in diamond nanostructures: Application to spin squeezing,” *Phys. Rev. Lett.* **110**, 156402 (2013).
- [80] David Petrosyan, Guy Bensky, Gershon Kurizki, Igor Mazets, Johannes Majer, and Jörg Schmiedmayer, “Reversible state transfer between superconducting qubits and atomic ensembles,” *Phys. Rev. A* **79**, 040304 (2009).
- [81] Xin Wang, Adam Miranowicz, Hong-Rong Li, and Franco Nori, “Method for observing robust and tunable phonon blockade in a nanomechanical resonator coupled to a charge qubit,” *Phys. Rev. A* **93**, 063861 (2016).
- [82] M. Tahir Naseem, André Xuereb, and Özgür E. Müstecaplıoğlu, “Thermodynamic consistency of the optomechanical master equation,” *Phys. Rev. A* **98**, 052123 (2018).
- [83] J.D. Cresser, “Thermal equilibrium in the jaynes-cummings model,” *J. Mod. Opt.* **39**, 2187–2192 (1992).
- [84] Werner Vogel and Dirk-Gunnar Welsch, *Quantum optics* (John Wiley & Sons, 2006).
- [85] M. G. A. Paris, “Quantum estimation for quantum technology,” *Int. J. Quantum Inf.* **7**, 125–137 (2009).
- [86] C. W. Helstrom, “Quantum detection and estimation theory,” (1969).
- [87] Samuel L. Braunstein and Carlton M. Caves, “Statistical distance and the geometry of quantum states,” *Phys. Rev. Lett.* **72**, 3439 (1994).
- [88] O. Pinel, P. Jian, N. Treps, C. Fabre, and D. Braun, “Quantum parameter estimation using general single-mode gaussian states,” *Phys. Rev. A* **88**, 040102 (2013).
- [89] Radim Filip and Petr Marek, “Thermally induced creation of quantum coherence,” *Phys. Rev. A* **90**, 063820 (2014).
- [90] Giacomo Guarneri, Michal Kolář, and Radim Filip, “Steady-state coherences by composite system-bath interactions,” *Phys. Rev. Lett.* **121**, 070401 (2018).
- [91] Alexander Holm Küllerich, Antonella De Pasquale, and Vittorio Giovannetti, “Dynamical approach to ancilla-assisted quantum thermometry,” *Phys. Rev. A* **98**, 042124 (2018).
- [92] M Tahir Naseem and Özgür E Müstecaplıoğlu, “Engineering entanglement between resonators by hot environment,” *Quantum Sci. Technol.* **7**, 045012 (2022).
- [93] J.R. Johansson, P.D. Nation, and Franco Nori, “Qutip: An open-source python framework for the dynamics of open quantum systems,” *Comput. Phys. Commun.* **183**, 1760–1772 (2012).